# A REAL-TIME LOW RESOLUTION RANGE-FINDER FOR ROBOTIC APPLICATIONS

**J. Forest[†], I. Rodríguez[†], J. Salvi[†] and E. Cabruja[‡]**

[†] Universitat de Girona, Institut d'Informàtica i Aplicacions
17003 Girona, Catalonia
email: forest,qsalvi,jmteixi@eia.udg.es

[‡] Centre Nacional de Microelectrònica - CSIC
08193 Cerdanyola del Vallès, Catalonia
email: enric@cnm.es

## Abstract

*A 5x5 photo-diode commercially available array has been used in order to build up a low-cost low resolution real-time range finder which is suitable for robotic applications like obstacle detection, since its purpose is to retrieve three-dimensional information from the close environment. The laser slit is detected by computing the time at which the image of the laser slit crosses the middle point between two consecutive neighbour photo-diodes. The time computation is made using digital timers, implemented in programmable logic devices (FPGAs). Programmable logic is used for the constant speed motor control and the communication with the host computer, as well. A calibration procedure is proposed in which very few constraints are needed, making the image sensor-laser arrangement geometry open, that is, the sensor and the laser can be positioned in almost any pose relative to each other.*

## 1 Introduction

Smart sensors are bringing computation to the sensor itself, instead of providing information to a separate processing step. This has led to a significant increase in the computation, permitting actual real-time applications to arise. Smart sensors are responsible of guiding missiles to the proper target, for instance. The computation is made at the pixel level, the row level, or even at the array level, bringing the contents of the pixels row by row or pixel by pixel, by means of a fast switching mechanism. (Kanade et al. 1991) and (Yokoyama et al. 1994) used the smart sensor approach in order to build up fast and accurate three-dimensional digitisers, by completely re-designing an image sensor, making the chip compute the time at which a constant speed rotating laser slit illuminates a point in the scene. Time illumination computation is equivalent to scanning angle synchronization if a constant speed rotating laser slit is used. In this work, a 5x5 photo-diode commercially available array has been used in order to build up a low-cost low resolution real-time range finder which is suitable for robotic

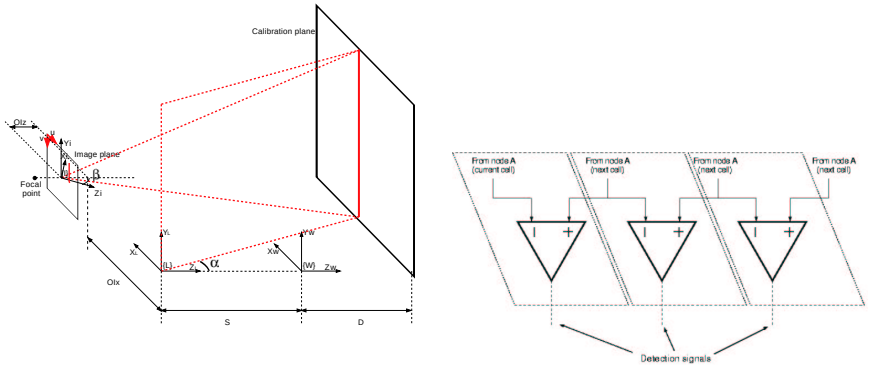


(a) (b)

Figure 1: Co-ordinate frames (a), and Detection circuit (b).

applications like obstacle detection, since its purpose is to retrieve three-dimensional information from the close environment. The laser slit detection is similar to that used by Yokohama, which computes the time at which the image of the laser slit crosses the middle point between two consecutive neighbour photo-diodes, although the time computation is made using digital timers, implemented in programmable logic devices (FPGAs). Programmable logic is used for the constant speed motor control and the communication with the host computer. A calibration procedure will be proposed in which very few constraints are needed, making the image sensor-laser arrangement geometry open, that is, the sensor and the laser can be positioned in almost any pose relative to each other.

## 2 Slit detection

Yokohama (Yokoyama et al. 1994) used two photo-sensitive areas in each of the pixels in the array, one of them being slightly bigger in area than the other. The slit detection was achieved by comparison between the voltage outputs of both neighbour photo-diodes, hence, a detection signal was triggered at the instant in which the peak light intensity falled onto the middle of the two photo-diodes. Figure 2a depicts the evolution of the two voltages with time, showing the instant of detection. In our approach, the photo-diodes in the array have been used in couples, such that four detection "points" exist in each row. Hence the two voltages to be compared have been taken from the two neighbour pixels in each couple. Figures 2b and 1b show one row of the array, in the common kathode configuration (by manufacture default) and a simple comparator circuit which provides the detection signal, respectively. In addition, an offset voltage has been added in one of the comparator inputs in order to cancel out thermal noise, avoiding false detections.

## 3 Calibration procecure

According to figure 1, the world co-ordinate frame is chosen to be placed in front of the $\{\mathrm{L}\}$ (laser) co-ordinate frame, with both $Z_L$ and $Z_W$ axis being coincident and the

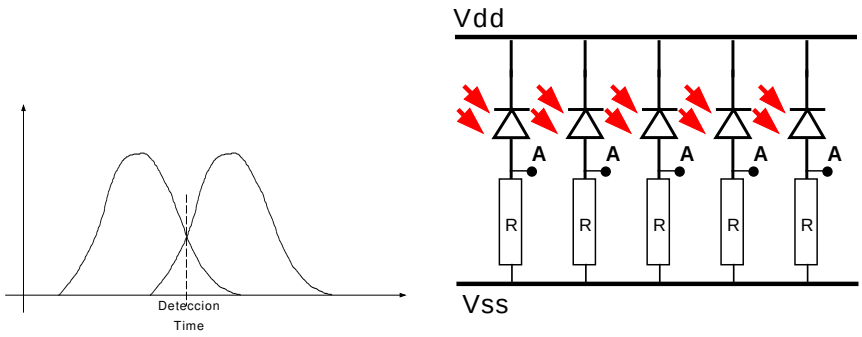


(a) (b)

Figure 2: Detection of laser slit by voltage comparison (a), and One row in common kathode. (b).

origins separated by OLz. The image sensor co-ordinate frame $\{\mathrm{I}\}$ is considered to be separated from $\{\mathrm{L}\}$ by OIx and OIz along the $X_L$ and $Z_L$ axis respectively. Note that the $X_C Z_C$ and $X_L Z_L$ planes are supposed to be coincident. In addition, $\{\mathrm{I}\}$ has a non-zero orientation angle ($\beta$) with respect to the $Z_W$ axe.

Assuming a pinhole model, a set of linear equations may be used in order to describe the behaviour of a camera, as stated and proved by (Faugeras 1993). The pinhole model is valid if no zoom or wide angle lenses are used, since these lenses introduce radial as well as tangential distorsion in the image, both of them non-linear effects. Since we are using a 50mm lens (a reflex camera body has been used as a housing for the 5x5 array), it is reasonable to assume this linear camera model for our purposes.

## 3.1 Camera model: intrinsic and extrinsic parameters

Any kind of discrete array-based video camera may be modelled in two stages, consisting in how the image points or pixels (in pixel co-ordinates) are related to an arbitrarily placed metric co-ordinate frame *-Intrinsic Parameters-*, and in how this metric co-ordinate frame is located with respect to an arbitrary world co-ordinate frame $\{\mathrm{W}\}$ *-Extrinsic Parameters-*.

The intrinsic parameters of a camera, assuming a pinhole model, are the focal distance ($f$), the principal point pixel co-ordinates ($u_0, v_0$) and the horizontal and vertical pixel pitch constants of proportionality ($K_u, K_v$). The reader is pointed to (Faugeras 1993) and (Salvi et al. 2002) to get deeper in camera calibration issues. In our case, though, we are not dealing with an already housed camera, but it is *the* camera what is being built, hence the horizontal and vertical constants of proportionality are supplied by the sensor manufacturer and the principal point must be well aligned with the optical axe of the lens, which is a mechanical issue, and has been chosen to be $(0, 0)$. Hence only $f$ must be estimated in the calibration procedure.

The estimation of the camera extrinsic parameters describe how the camera itself (or more concretely, the camera co-ordinate frame) is located with respect to the world co-ordinate frame. In our case, only the X (OIx) and Z (OIz) co-ordinates have been assumed to be variable (i.e. unknown a priori), since $Y_C$ has been assumed to be parallel to both $Y_L$ and $Y_W$. This assumption may be adopted if the laser plane emitter is perfectly vertical with respect to $Y_L$.

## 3.2 Calibration equations

The position and orientation of {I} with respect to {W} is described by the homogeneous transformation shown in equation 1, hence, the point co-ordinates of the focal point, expressed as ${}^{I}FP = [0, 0, -f, 1]^T$ with respect to {I}, is obtained with respect to {W} making ${}^{W}FP = {}^{W}T_I \cdot {}^{I}P$, yielding the expression of equation 2.

$$ {}^{W}T_I = \begin{bmatrix} cos(\beta) & 0 & sin(\beta) & OIx \\ 0 & 1 & 0 & 0 \\ -sin(\beta) & 0 & cos(\beta) & OIz \\ 0 & 0 & 0 & 1 \end{bmatrix} \tag{1} $$

$$ {}^{W}FP = \begin{bmatrix} OIx - f \cdot sin(\beta) \\ 0 \\ OIz - f \cdot cos(\beta) \\ 1 \end{bmatrix} \tag{2} $$

Once the focal point is expressed with respect to {W}, each of the detection point locations will be used in order to get the direction vectors (equation 3) which, together with ${}^{W}FP$, yield the expression of equation 4, which is the line-of-sight equation in parametric form for each detection point, where $R_X, R_Y, R_Z$ are the co-ordinates of the line-of-sight points, $nx, ny$ are the pixel co-ordinates of each detection point, with respect to {I}, and $dx, dy$ are the pixel pitch in the horizontal and vertical directions respectively. The pixel pitch is the inverse of the pixel pitch constant of proportionality $(K_u, K_v)$. As can be seen in equation 4, $R_Y$ is dependent only on the Y co-ordinate in pixels ($ny$) and the pixel vertical pitch ($py$). This is due to the fact that there is no *vertical* information provided by the laser scan, since the laser shape is a vertical plane, which projects a slit parallel to the $Y_W$ axe. Hence, the measurement error in the Y direction is $\pm$7.5mm at a 500mm range, independently of the scanning mechanism, if the vertical detection point is assumed to fall in the centre of the pixels. Clearly, this shows that in order to minimise the reconstruction errors in the vertical, or Y, direction it is recommended that the pixels have the vertical pitch as short as possible.

$$ V_d^W = \begin{bmatrix} nx \cdot dx \cdot cos(\beta) - f \cdot sin(\beta) \\ ny \cdot dy \\ nx \cdot dx \cdot sin(\beta) - f \cdot cos(\beta) \\ 0 \end{bmatrix} \tag{3} $$

$$ \begin{bmatrix} R_x \\ R_y \\ R_z \\ 1 \end{bmatrix} = \lambda \cdot \begin{bmatrix} nx \cdot dx \cdot cos(\beta) - f \cdot sin(\beta) \\ ny \cdot dy \\ nx \cdot dx \cdot sin(\beta) - f \cdot cos(\beta) \\ 0 \end{bmatrix} + \begin{bmatrix} OIx - f \cdot sin(\beta) \\ 0 \\ OIz - f \cdot cos(\beta) \\ 1 \end{bmatrix} \tag{4} $$

In order to get the reconstruction (or estimated three-dimensional co-ordinates) of a point contained in a line-of-sight, it is necessary to obtain the point intersection of the laser plane with the line-of-sight itself. Hence, the laser plane equation must be obtained in terms of $\alpha$, the scanning angle. ${}^{L}O = [0, 0, 0, 1]^T$ is the laser rotation centre point with respect to {L}. Since the orientation of {L} has chosen to be equal to the orientation of {W}, and its position is $-S$ mm away from the origin of {W} along $Z_W$, equation 5 expresses ${}^{W}T_L$ by means of a homogeneous transformation. Hence, the laser rotation point (it is a rotation *axe*, indeed, but a *point* has been chosen for

notation convenience only), can be found with respect to {W} by left-multipliying ${}^{L}O$, such that ${}^{W}O = {}^{W}T_{L} \cdot {}^{L}O$, and its expression is shown in equation 6.

$$ {}^{W}T_{L} = \begin{bmatrix} 1 & 0 & 0 & 0 \\ 0 & 1 & 0 & 0 \\ 0 & 0 & 1 & -S \\ 0 & 0 & 0 & 1 \end{bmatrix} \tag{5} $$

$$ {}^{L}O = \begin{bmatrix} 0 \\ 0 \\ -S \\ 1 \end{bmatrix} \tag{6} $$

The normal vector which describes the laser plane orientation may be obtained by left-multipliying the normal vector expression when $\alpha = 0$, by a rotation homogeneous transformation upon the $Y_L$ axe, as it is expressed in equation 7. In addition, if $V_n^L$ is left-multiplied by ${}^{W}T_{L}$, the normal vector expression with respect to {W} is obtained, as shown in equation 8. Since the orientation of {L} and {W} are equal, there have been no changes in the normal vector expression. Once both the normal vector and a point of the laser plane (which has been chosen to be the rotation centre for convenience) have been found, the laser plane equation in terms of $\alpha$ is configured, and its expression is shown in equation 9.

$$ V_n^L = \begin{bmatrix} cos(\alpha) & 0 & sin(\alpha) & 0 \\ 0 & 1 & 0 & 0 \\ -sin(\alpha) & 0 & cos(\alpha) & 0 \\ 0 & 0 & 0 & 1 \end{bmatrix} \cdot \begin{bmatrix} 1 \\ 0 \\ 0 \\ 0 \end{bmatrix} = \begin{bmatrix} cos(\alpha) \\ 0 \\ -sin(\alpha) \\ 0 \end{bmatrix} \tag{7} $$

$$ V_n^W = \begin{bmatrix} 1 & 0 & 0 & 0 \\ 0 & 1 & 0 & 0 \\ 0 & 0 & 1 & -S \\ 0 & 0 & 0 & 1 \end{bmatrix} \cdot \begin{bmatrix} cos(\alpha) \\ 0 \\ -sin(\alpha) \\ 0 \end{bmatrix} = \begin{bmatrix} cos(\alpha) \\ 0 \\ -sin(\alpha) \\ 0 \end{bmatrix} \tag{8} $$

$$ X \cdot cos(\alpha) - Z \cdot sin(\alpha) = S \cdot sin(\alpha) \tag{9} $$

Once both the parametric equation of the line-of-sight and the laser plane equation have been found, a system of 4 linear equations can be set, but there is still a fifth equation which must be considered in order to obtain the calibration parameters. The calibration parameters are $\beta$, $S$, $OIx$, $OIz$ and $f$, and they must be obtained from the knowledge of a calibration target object, which is, in our case, a plane located at known distances along the $Z_W$ axe and parallel to the $X_W Y_W$ plane. Hence the fifth equation of the linear system is $Z = d_i$, where $d_i$ is the distance of the i-th plane to the origin of {W}, as shown in equations 10.

$$ \begin{cases} (1) X \cdot cos(\alpha) - Z \cdot sin(\alpha) = S \cdot sin(\alpha) \\ (2) X = \lambda \cdot (nx \cdot dx \cdot cos(\beta) - f \cdot sin(\beta)) + OIx - f \cdot sin(\beta) \\ (3) Y = \lambda \cdot ny \cdot dy \\ (4) Z = \lambda \cdot (-nx \cdot dx \cdot sin(\beta) - f \cdot cos(\beta)) + OIz - f \cdot cos(\beta) \\ (5) Z = d_i \end{cases} \tag{10} $$

If $\lambda$ is isolated from the 10(2) and 10(4) equations, two expressions for $\lambda$ are obtained. If these two expressions are equated, the line-of-sight equation in the plane $X_W Z_W$

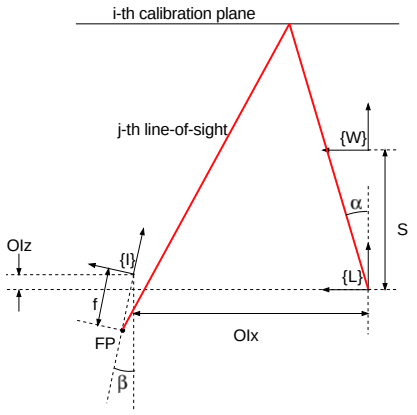


Figure 3: Intersection between a line-of-sight and the laser plane.

is obtained, as shown in equation 11. Note that it is senseless to consider the line-of-sight equation in the vertical direction, since it does not contribute any additional information for obtaining the calibration parameters.

$$\begin{aligned} &Z \cdot (nx \cdot dx \cdot cos(\beta) - f \cdot sin(\beta)) + X \cdot (nx \cdot dx \cdot sin(\beta) + f \cdot cos(\beta)) + \\ &+OIz \cdot (f \cdot sin(\beta) - nx \cdot dx \cdot cos(\beta)) - OIx \cdot (f \cdot cos(\beta) + nx \cdot dx \cdot sin(\beta)) + \\ &+f \cdot nx \cdot dx = 0 \end{aligned} \tag{11}$$

If 10(5) is substituted into 10(1) and 11, a new system of 2 linear equations is obtained, which, after isolating X in both of them and equating, equation 12 is obtained, where the only unknowns are the calibration parameters.

$$\begin{aligned} &OIz - OIx \cdot tan(\beta) + nx \cdot dx \cdot (OIz \cdot \tfrac{tan(\beta)}{f} + OIx \cdot \tfrac{1}{f} - sec(\beta)) - \\ &-nx \cdot dx \cdot d_i \cdot \tfrac{1}{f} + d_i \cdot tan(\beta) - nx \cdot dx \cdot d_i \cdot tan(\alpha) \cdot \tfrac{tan(\beta)}{f} - \\ &-nx \cdot dx \cdot tan(\alpha) \cdot \tfrac{tan(\beta) \cdot S}{f} - tan(\alpha) \cdot S = d_i \cdot tan(\alpha) \end{aligned} \tag{12}$$

## 3.3 Obtaining the calibration parameters

In order to obtain the calibration parameters ($\beta$, $S$, $OIx$, $OIz$ and $f$), several complete scans on the calibration plane at different ranges must be made. In these scans, all the detection points **in a row** must detect the scanning stripe projected on the calibration plane. A complete scan will detect the scanning *times* in which the stripe *cuts* each of the line-of-sights, hence, in a given instant of time, when the stripe illuminates the **i-th** calibration plane, the laser light will intersect the **j-th** line-of-sight, as shown in figure 3. Using *i* and *j* as the plane and line-of-sight indices, equation 12 can be arranged as shown in equation 13.

Table 1: Metric errors due to electric noise.

| **Zw(mm)** | 10 | 110 | 210 | 310 |
|---|---|---|---|---|
| **dX(um)** | $4.37e01$ | $1.08e01$ | $2.93e01$ | $5.53e01$ |
| **dZ(um)** | $4.93e01$ | $1.21e01$ | $3.31e01$ | $6.24e01$ |

$$\begin{bmatrix} \vdots & \vdots & \vdots & \vdots & \vdots & \vdots & \vdots \\ 1 & dx \cdot n_j & -dx \cdot d_i \cdot n_j & d_i - & dx \cdot d_i \cdot n_j \cdot tan(\alpha_{ij}) & -dx \cdot n_j \cdot tan(\alpha_{ij}) & -tan(\alpha_{ij}) \\ \vdots & \vdots & \vdots & \vdots & \vdots & \vdots & \vdots \end{bmatrix} \cdot \cdot \begin{bmatrix} OIz - OIx \cdot tan(\beta) \\ OIz \cdot \frac{tan(\beta)}{f} + OIx \cdot \frac{1}{f} - \frac{1}{cos(\beta)} \\ \frac{1}{f} \\ tan(\beta) \\ \frac{tan(\beta)}{f} \\ S \cdot \frac{tan(\beta)}{f} \\ S \end{bmatrix} = \begin{bmatrix} \vdots \\ d_i tan(\alpha_{ij}) \\ \vdots \end{bmatrix} \tag{13}$$

In order to solve the unknowns, a minimum of 7 *detections* or points should be provided for satisfiying all the constraints, but since any real image capture system is noisy, according to (Hartley & Zisserman 2000), it is much more advisable to include many more points so an overdetermined set of equations can be solved minimising some cost function. In our simulation, the calibration plane has been scanned at 4 different ranges, obtaining 4 points per scan, which yields a total of 16 points. In addition, since it has been proved sufficient above, only the row at $Y_I = 0$ has been used, and the singular value decomposition method has been utilised in order to solve the set of linear equations.

If the unknowns column vector is called *U*, with components $U_1 \ldots U_7$, the expressions of the calibration parameters can be obtained from 13, as shown in equation 14. The real parameters and the estimated ones do not show to be appretiably different, and their values in our simulation are: $\beta = 15^o$, $S = 200$ mm, $OIz = 20$ mm, $OIx = 400$ mm and $f = 50$ mm.

$$\begin{aligned} \beta &= atan(U_4) \\ S &= U_7 \\ f &= \tfrac{1}{U_3} \\ OIz &= \tfrac{U_2 - U_1 U_3 U_4 + sec(\beta)}{U_3 (1 + U_4^2)} \\ IOx &= U_1 + OIz \cdot U_4 \end{aligned} \tag{14}$$

## 3.4 Simulation results

Table 1 show the results of the reconstruction of a plane for different ranges, whith no errors due to quantisation. The error due to quantisation becomes smaller and smaller as the number of quantisation bits increase, but when using 16 bits or more, errors due to electrical noise become more important, hence, it does not make sense to include more than 24 bits, for the quantisation, since, as can be seen in table 2, the errors stabilise for 16, 24 and 32 bits.

Table 2: Metric errors due to both electric and quantisation noise.

| | **Zw(mm)** | 10 | 110 | 210 | 310 |
|---|---|---|---|---|---|
| 8 bits | **dX(um)** | $1.73e03$ | $1.19e03$ | $2.47e03$ | $3.73e03$ |
| | **dZ(um)** | $1.88e03$ | $1.94e03$ | $3.05e03$ | $4.03e03$ |
| 16 bits | **dX(um)** | $8.53e00$ | $6.69e-01$ | $1.42e01$ | $4.76e01$ |
| | **dZ(um)** | $9.62e00$ | $2.91e00$ | $1.60e01$ | $5.36e01$ |
| 24 bits | **dX(um)** | $4.20e-01$ | $1.03e01$ | $2.82e01$ | $5.29e01$ |
| | **dZ(um)** | $4.47e-01$ | $1.16e01$ | $3.17e01$ | $5.97e01$ |
| 32 bits | **dX(um)** | $4.37e-01$ | $1.08e01$ | $2.93e01$ | $5.53e01$ |
| | **dZ(um)** | $4.93e-01$ | $1.21e01$ | $3.31e01$ | $6.24e01$ |

# References


Faugeras, O. (1993). *Three-Dimensional Computer Vision: A Geometric Viewpoint*, The MIT Press.

Hartley, R. & Zisserman, A. (2000). *Multiple view geometry*, Cambridge University Press.

Kanade, T., Gruss, A. & Carley, L. (1991). A very fast vlsi rangefinder, *Proc. IEEE International Conference on Robotics and Automation*, Vol. 2, pp. 1322–1329.

Salvi, J., Armangué, X. & Batlle, J. (2002). A comparative review of camera calibrating methods with accuracy evaluation, *Pattern Recognition* **35**(7): 1617–1635.

Yokoyama, A., Sato, K., Yoshigahara, T. & Inokuchi, S. (1994). Realtime range imaging using adjustment-free photo-vlsi, *Proceedings of the IEEE/RSJ International Conference on Intelligent Robots and Systems*, pp. 1751–1758.